BMC Genomics

RESEARCH

Open Access

Differential chromatin accessibility and Gene Expression Associated with Backfat Deposition in pigs

Zhe Zhang[1], Lebin Chang[1], Bingjie Wang[1], Yilin Wei[1], Xinjian Li[1,2], Xiuling Li[1], Yongqian Zhang[3], Kejun Wang[1], Ruimin Qiao[1], Feng Yang[1], Tong Yu[1] and Xuelei Han[1*]

Abstract

Background Backfat serves as a vital fat reservoir in pigs, and its excessive accumulation will adversely impact pig growth performance, farming efficiency, and pork quality. The aim of this research is to integrate assay for transposase-accessible chromatin with high-throughput sequencing (ATAC-seq) and RNA sequencing (RNA-seq) to explore the molecular mechanisms underlying porcine backfat deposition.

Results ATAC-seq analysis identified 568 genes originating from 698 regions exhibiting differential accessibility, which were significantly enriched in pathways pertinent to adipocyte differentiation and lipid metabolism. Besides, a total of 283 transcription factors (TFs) were identified by motif analysis. RNA-seq analysis revealed 978 differentially expressed genes (DEGs), which were enriched in pathways related to energy metabolism, cell cycle and signal transduction. The integration of ATAC-seq and RNA-seq data indicates that DEG expression levels are associated with chromatin accessibility. This comprehensive study highlights the involvement of critical pathways, including the Wnt signaling pathway, Jak-STAT signaling pathway, and fatty acid degradation, in the regulation of backfat deposition. Through rigorous analysis, we identified several candidate genes (*LEP*, *CTBP2*, *EHHADH*, *OSMR*, *TCF7L2*, *BCL2*, *FGF1*, *UCP2*, *CCND1*, *TIMP1*, and *VDR*) as potentially significant contributors to backfat deposition. Additionally, we constructed TF-TF and TF-target gene regulatory networks and identified a series of potential TFs related to backfat deposition (FOS, STAT3, SMAD3, and ESR1).

Conclusions This study represents the first application of ATAC-seq and RNA-seq, affording a novel perspective into the mechanisms underlying backfat deposition and providing invaluable resources for the enhancement of pig breeding programs.

Keywords ATAC-seq, RNA-seq, Backfat deposition, Regulatory mechanisms, Yunong Black Pig, Duroc Pig

Introduction

Adipose tissue is pivotal in energy storage and metabolism within animals [1]. It can be classified into subcutaneous fat and visceral fat according to its position [2]. And its growth results from the increase in both the size and number of adipocytes [3]. Mature adipocytes derive from the proliferation and differentiation of multipotent mesenchymal stem cells [4]. Notably, triglyceride accumulation initially enlarges existing adipocytes, triggering the generation of new adipocytes

*Correspondence:
Xuelei Han
hxl014@126.com
[1] College of Animal Science and Technology, Henan Agricultural University, Zhengzhou 450046, China
[2] Sanya Institute, Hainan Academy of Agricultural Science, Sanya 572025, China
[3] Henan Yifa Animal Husbandry Co., Ltd, Hebi 458000, China

upon reaching their size limit [5]. Backfat thickness is a significant trait affecting the economic efficiency of pig production and reproductive performance [6]. With rising living standards, consumer preference has shifted towards quality over quantity with lean meat products being more favored, emphasizing the importance of reducing backfat and enhancing lean meat yield to meet market demands and improve profitability. The Yunong black pig (YN), renowned for its high fertility, rapid growth, superior meat quality and robust adaptability, is a locally cultivated breed in China [7]. However, compared to Duroc pig (D), YN exhibits a thicker backfat, rendering them ideal models to investigate the molecular mechanisms underlying differential backfat deposition.

Chromatin accessibility, a crucial aspect of epigenetics, represents the direct impact of chromatin structure on gene transcription [8]. That is to say, when the binding affinity between histones and DNA increases, a dense nucleosome structure forms, preventing transcription factors (TFs) from binding to cis-regulatory elements on DNA. Conversely, reduced histone-DNA affinity results in a looser nucleosome structure, facilitating the binding of TFs to cis-regulatory elements [9, 10]. The assay for transposase-accessible chromatin with high-throughput sequencing (ATAC-seq), widely used in studying various cis-regulatory elements and predicting TF binding sites, is a powerful technology for identifying open chromatin regions [11]. The combination of ATAC-seq and RNA sequencing (RNA-seq) technologies enables the simultaneous acquisition of information on chromatin accessibility and downstream gene expression, thereby revealing the complex networks of gene expression regulation [12]. This combined approach has been successfully employed in numerous studies to identify key factors involved in diverse biological processes [13–15].

Herein, this study aims to investigate the molecular mechanisms underlying porcine backfat deposition by leveraging ATAC-seq and RNA-seq to understand chromatin accessibility and gene expression profiles in YN and D backfat tissues. Through ATAC-seq, we identified differences in chromatin accessibility between these two breeds while RNA-seq revealed that in the gene expression. By integrating ATAC-seq and RNA-seq data, we delved into the regulatory and expression patterns of differentially expressed genes (DEGs) and their open chromatin regions, highlighting potential TFs and core genes involved in fat deposition regulation. These findings deepen our understanding of the genetic and epigenetic mechanisms underlying backfat deposition, setting the stage for future investigations into its molecular mechanisms.

Materials and methods

Animals and sample collection

The experimental animals comprised YN and D sourced from the farm of Henan Yifa Animal Husbandry Co., Ltd, all reared under identical conditions. Upon reaching a weight of 115.00 ± 5.00 kg, the animals were stunned by electric shock followed by slaughter in an unconscious state, and their backfat tissue was promptly transferred to liquid nitrogen and then stored at -80 °C for subsequent experiments.

Histological analysis

To access adipocyte size, fresh adipose tissue samples were initially fixed in a 4% paraformaldehyde solution for 24 h prior to paraffin embedding and then were sectioned after solidification. After staining with hematoxylin and eosin (H&E), the sections were subsequently sealed with neutral resin. Digital scanning of the sections was performed using a digital slice scanner. CaseViewer (C.V2.4) software was utilized to randomly select visual fields at 100x magnification. Subsequently, ImageJ, an image analysis software, was used to randomly sample morphologically intact cells and measure the area of adipocytes in the captured images [16].

ATAC-seq and analysis

Three biological replicates were used. The Agilent 2100 Bioanalyzer was used to check the library fragment size and concentration. Upon passing quality control, 150 bp paired-end sequencing was performed using the Illumina NovaSeq 6000 [17]. Raw sequencing data underwent quality control with cutadapt (V2.5), involving the removal of adapter sequences, low-quality bases, and sequences with a high proportion of unknown bases from the raw sequencing data, as well as reads shorter than 5 bp after the aforementioned quality control steps. Clean reads were aligned to the reference genome (Sus scrofa 11.1) using Bowtie2 (V2.3.4.1) with specific parameters: "-X2000 --mm --local --threads 6" [18]. Low-quality alignments, mitochondrial genome alignments, and redundant sequences introduced by PCR were filtered out. After library and sequencing data quality control, MACS2 (V2.1.1) software was used to identify ATAC-seq enrichment peaks, mapping out open chromatin regions across the entire genome for each sample. The parameters used were: "-p 0.01 --nomodel --shift −75 --extsize 150 -B --SPMR --keep-dup all --call-summits" [19]. ChIPseeker (V1.32.1) was used to evaluate the distribution of peaks in various functional regions of the genome and annotate associated genes [20]. Differential peaks were identified using the DESeq2 (V1.36.0) package in R based on the conditions: p-value < 0.05 and |log2(fold change)| ≥ 1 [21]. Volcano plots were generated using the

online bioinformatics visualization platform provided by WeSeq (https://www.bioinformatics.com.cn/). To identify enriched motifs in the genomic regions of differential peaks, the findMotifsGenome.pl script from the HOMER suite was utilized. Protein-protein interactions (PPI) among TFs were analyzed using the Search Tool for the Retrieval of Interacting Genes/Proteins (STRING) database (http://string-db.org), considering interactions with a score above 0.4. Subsequently, visualization was performed using Cytoscape software [22].

RNA-seq and analysis

The Fastp (V0.23.2) software was utilized for quality control of the raw data, generating high-quality clean reads. These reads were subsequently aligned to the reference genome (Sus scrofa 11.1) using HISAT2 (V2.2.1) software with specific parameters: "--dta --phred33 -p 4 --known-splicesite-infile" [23]. FeatureCounts (V2.0.3) was then utilized to quantify the reads aligned to the reference genome (Sus scrofa 11.1), applying the parameters: "-p --countReadPairs -T 2 -t exon -g gene_id" to accurately assign reads to their corresponding genes. To eliminate the influence of sequencing depth and gene length on expression calculation, the read counts were normalized using the Fragments Per Kilobase of transcript per Million mapped reads (FPKM) method. DESeq2 (V1.36.0) was employed to analyze DEGs between groups [24], adopting a threshold of $|\log2(\text{fold change})| \geq 1$ and p-value < 0.05 as criteria for statistical significance. Gene set enrichment analysis (GSEA) was performed using the OmicShare tools (https://www.omicshare.com/tools), with statistical significance attributed to pathway exhibiting |NES| > 1, NOM p-value < 0.05, FDR q-value < 0.25.

Integration analysis of ATAC-seq and RNA-seq

To compare the differential peak associated genes by ATAC-seq to the DEGs by RNA-seq, the overlapping genes were identified. These overlapping genes were then subjected to correlation analysis to examine the relationship between chromatin accessibility and gene expression levels. Furthermore, Gene Ontology (GO) and Kyoto Encyclopedia of Genes and Genomes (KEGG) pathway enrichment analyses were conducted on these overlapping genes. The transcriptional regulatory relationships between TFs and target genes were obtained from the Transcriptional Regulatory Relationships Unraveled by Sentence-based Text Mining database (TRRUST; https://www.grnpedia.org/trrust/).

GO and KEGG pathway analyses of differential genes

KEGG pathway enrichment analysis was conducted on the differential genes using KOBAS (http://bioinfo.org/kobas). Pathways were deemed enriched if they surpassed a statistical significance threshold of p-value < 0.05. The resulting enriched pathways were visualized using OmicShare tools (https://www.omicshare.com/tools).

Real-time fluorescence quantitative PCR

To validate the RNA-seq data, seven DEGs were randomly selected from both the D and YN groups for Real-time fluorescence quantitative PCR (RT-qPCR). The primer information is shown in Table S13. RNA extracted from backfat was reverse-transcribed into cDNA using the Evo M-MLV RT Kit with gDNA Clean for qPCR (AG11705, Accurate Biotechnology (Hunan) Co., Ltd, Changsha, China). q-PCR was performed on the CFX96 real-time PCR detection system (Bio-Rad, Hercules, CA, USA) using the SYBR Green Premix Pro Taq HS qPCR Kit (AG11701, Accurate Biotechnology (Hunan) Co., Ltd, Changsha, China), following the provided guidelines. GAPDH served as the internal control gene to normalize gene expression levels and the relative gene expression was calculated using the $2^{-\Delta\Delta Ct}$ method.

Result

Histological analysis of backfat tissues in Yunong black pigs and duroc pigs

The paraffin parts of backfat tissues from YN and D revealed a significantly larger adipocytes in YN compared to D (P < 0.001; Fig. 1A and B). Subsequently, further experiments are performed utilizing these two sets of backfat tissues.

Characteristics of chromatin accessibility of backfat tissues in Yunong black pigs and duroc pigs

To investigate the mechanisms behind the differences in backfat thickness, ATAC-seq was used to examine the differences in genome-wide chromatin accessibility between YN and D backfat tissues. A total of 481,524,838 raw reads were obtained from the D group and 468,242,734 raw reads from the YN group. Following rigorous filtering, the respective counts of clean reads amounted to 481,506,340 and 468,224,222, with over 97% of these reads from each sample successfully mapped to the reference genome (Sus scrofa 11.1; Table S1). Analysis of the length of inserted fragments produced across libraries was consistent with the expected distribution, with the most prominent peak on the left side representing nucleosome-free fragments in open chromatin regions, while peaks around 200 bp and 400 bp on the right side corresponded to open chromatin regions containing one and two nucleosome fragments, respectively (Fig. 2A). Chromosomal peak distribution plots demonstrated consistency in both genomic signal and peak patterns across the two sets of chromosomes (Fig. 2B). Sequences uniquely aligned to the reference genome

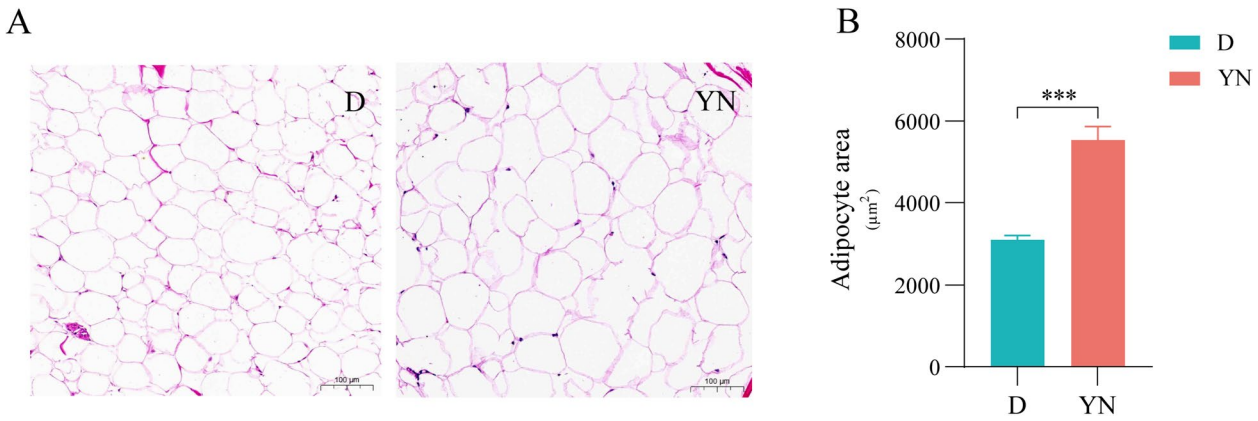

Fig. 1 Histological analysis of backfat tissues. **A** 100x magnification of backfat tissues of YN and D. **B** Adipocyte area of backfat tissues of YN and D. mean ± SEM, *** $P < 0.001$

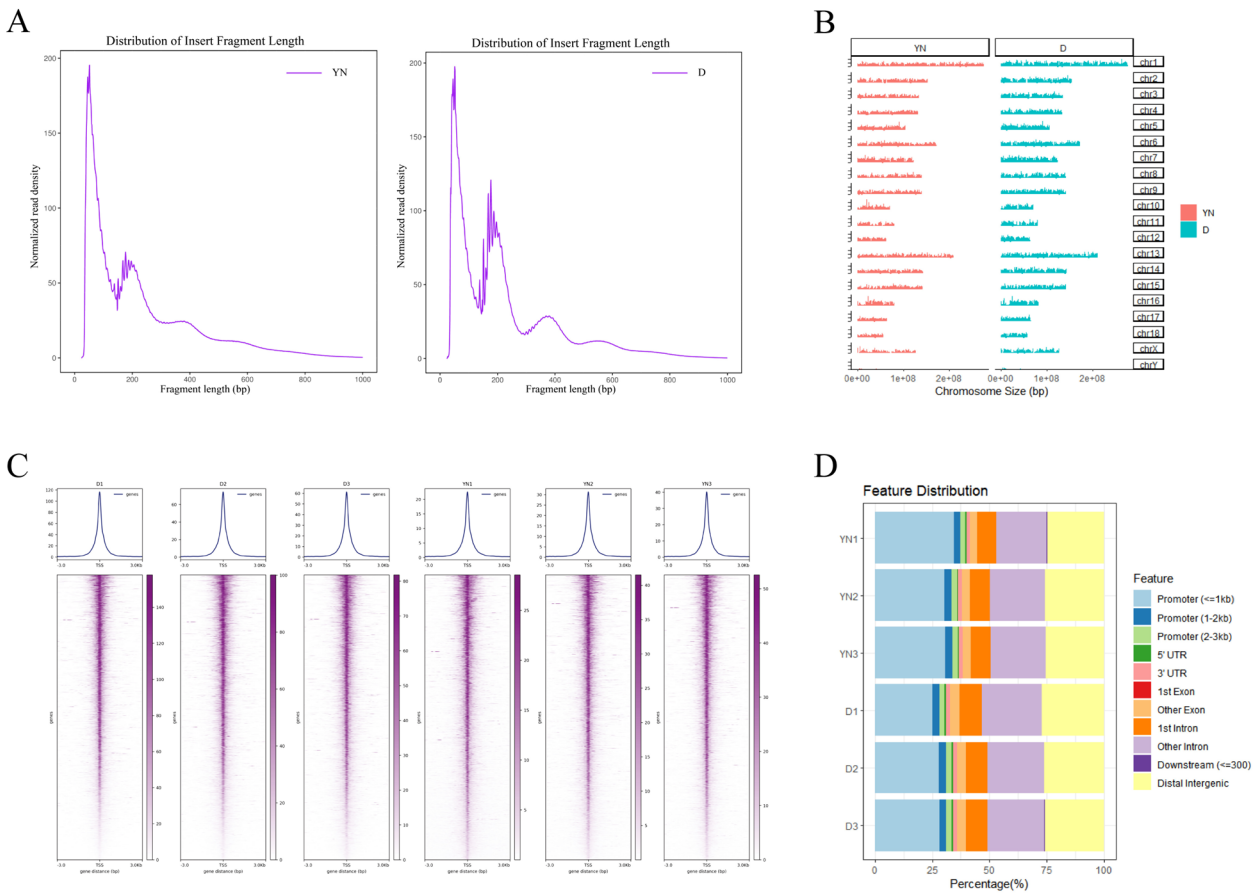

Fig. 2 ATAC-seq quality control and analyses of the peaks. **A** Distribution of inserted fragment length. **B** Distribution of peaks on the chromosomes. **C** ATAC-seq signal enrichment within 3 kb upstream and downstream of the TSS. **D** Peak distribution across various genomic regions.

were enriched within a 3 kb range around the gene transcription start site (TSS). Notably, a distinct enrichment of sequencing reads was observed in proximity to TSS, underscoring the high quality of the ATAC-seq data (Fig. 2C). All peaks were annotated, and the results showed that most were mapped to promoters, introns, and distal intergenic regions (Fig. 2D).

Differential chromatin accessibility and motif analysis of backfat tissues in Yunong black pigs and Duroc pigs

To determine the open chromatin regions associated with backfat deposition, differential chromatin accessibility analysis was conducted on the YN and D groups. Principal component analysis (PCA) underscored the robust intra-group reproducibility and distinct inter-group variations across the samples (Fig. 3A). The differential analysis identified 698 differential peaks in the YN group compared to the D group, with 160 down-regulated and 538 up-regulated peaks (Fig. 3B, Table S2). Annotation of these differential peaks revealed a total of 568 associated genes (Table S3). The enriched GO terms for these genes mainly included cellular developmental process, cell differentiation, developmental process and cell development, etc. (Fig. 3C, Table S4). KEGG pathway enrichment analysis of these genes identified 55 significantly enriched pathways (Table S5), with the top 10 pathways related to cellular metabolism, calcium and phosphate homeostasis, lipid metabolism, and cell signaling, including Metabolic pathways, Sphingolipid metabolism, and PPAR signaling pathway (Fig. 3D). These results suggest that chromatin accessibility-induced transcriptional changes play a vital role in modulating the extent of backfat deposition. A total of 283 TFs were identified through motif analysis (p-value < 0.01; Table S6), with a notable enrichment of key TFs implicated in adipocyte differentiation and lipid metabolism. Specifically, FOS, ATF3, AP-1, and CEBP emerged as significantly enriched TFs, with FOS being the most enriched (Fig. 3E). Additionally, the TF interaction network underscores FOS, STAT3, ESR1, and SMAD3 as the top four hub TFs most closely connected with other TFs, particularly FOS exhibiting the most prominent interactions (Fig. 3F). This indicates that the differences in lipid deposition levels are associated with the binding of these TFs to open chromatin regions.

Gene expression profiling of backfat tissues in Yunong black pigs and duroc pigs

To assess the gene expression patterns in the YN and D groups, RNA-seq analysis was conducted on their backfat tissues. The D group and YN group obtained 232,432,430 and 259,067,582 raw reads, respectively. After filtering, the number of clean reads for the D and YN groups was 229,840,268 and 256,158,910, respectively. Notably, over 96% of these clean reads from each sample were mapped to the reference genome (Sus scrofa 11.1; Table S7). PCA revealed correlations among the three biological replicates of YN and D groups (Fig. 4A). To identify functional genes involved in fat deposition, 978 DEGs were identified, with 396 genes down-regulated and 582 genes up-regulated in the YN group compared to the D group (Fig. 4B, Table S8). GO enrichment analysis showed that DEGs are primarily enriched in terms including system development, multicellular organism development, cell differentiation, and cellular developmental process (Fig. 4C, Table S9). KEGG pathway enrichment analysis of the DEGs identified 86 significantly enriched pathways (Table S10). Among the top 10 pathways, the enrichment of Metabolic pathways, Biosynthesis of amino acids, ECM-receptor interaction, Carbon metabolism pathways, and p53 signaling pathway highlights the involvement of these DEGs in maintaining cellular and tissue homeostasis, as well as regulating metabolic processes (Fig. 4D). To gain a deeper understanding of the expression patterns and functions of all genes, the gene set enrichment analysis (GSEA) was performed. Consistently, the Biosynthesis of amino acids and Carbon metabolism pathways emerged as significantly enriched. Additionally, notable enrichments were also observed in the Jak-STAT signaling pathway and Fatty acid metabolism (Fig. 4E).

Integration analysis of ATAC-seq and RNA-seq

The integrated analysis of differential genes from ATAC-seq and RNA-seq data was conducted. Through data alignment, a total of 39 overlapping genes were identified (Fig. 5A, Table S11). Correlation analysis showed a significant positive relationship between the chromatin accessibility of these overlapping genes and their expression levels (Fig. 5B). To further elucidate the functions of these genes, GO and KEGG enrichment analyses were conducted. GO enrichment analysis revealed enrichment in terms including filamin binding, positive regulation of intracellular protein transport, positive regulation of p38MAPK and stress-activated MAPK cascades (Fig. 5C, Table S12). KEGG enrichment analysis showed that these genes participate in diverse pathways, including the Jak-STAT signaling pathway, Wnt signaling pathway, and Fatty acid degradation. These pathways are notably associated with cell proliferation and differentiation, signal transduction, and lipid metabolism (Fig. 5D, Table S13). By predicting target genes, 164 target genes of FOS, STAT3, ESR1, and SMAD3 were identified (Table S14). Comparing these target genes with DEGs resulted in 15 overlapping genes (Fig. 5E and F; Table 15), many of which are associated with lipid metabolism, energy balance, adipogenesis, and lipolysis, such as *LEP*, *FGF1*, *VDR* and *BCL2*.

Validation of RNA-seq results using RT-qPCR

To confirm RNA-seq results, RT-qPCR was conducted on seven randomly selected DEGs (*ADH1C*, *HIF1A*, *LIPE*, *NPTX1*, *PRSS35*, *STAT3* and *UCHL1*). The findings demonstrated that RT-qPCR gene expression patterns aligned with RNA-seq data, validating its accuracy (Fig. 6).

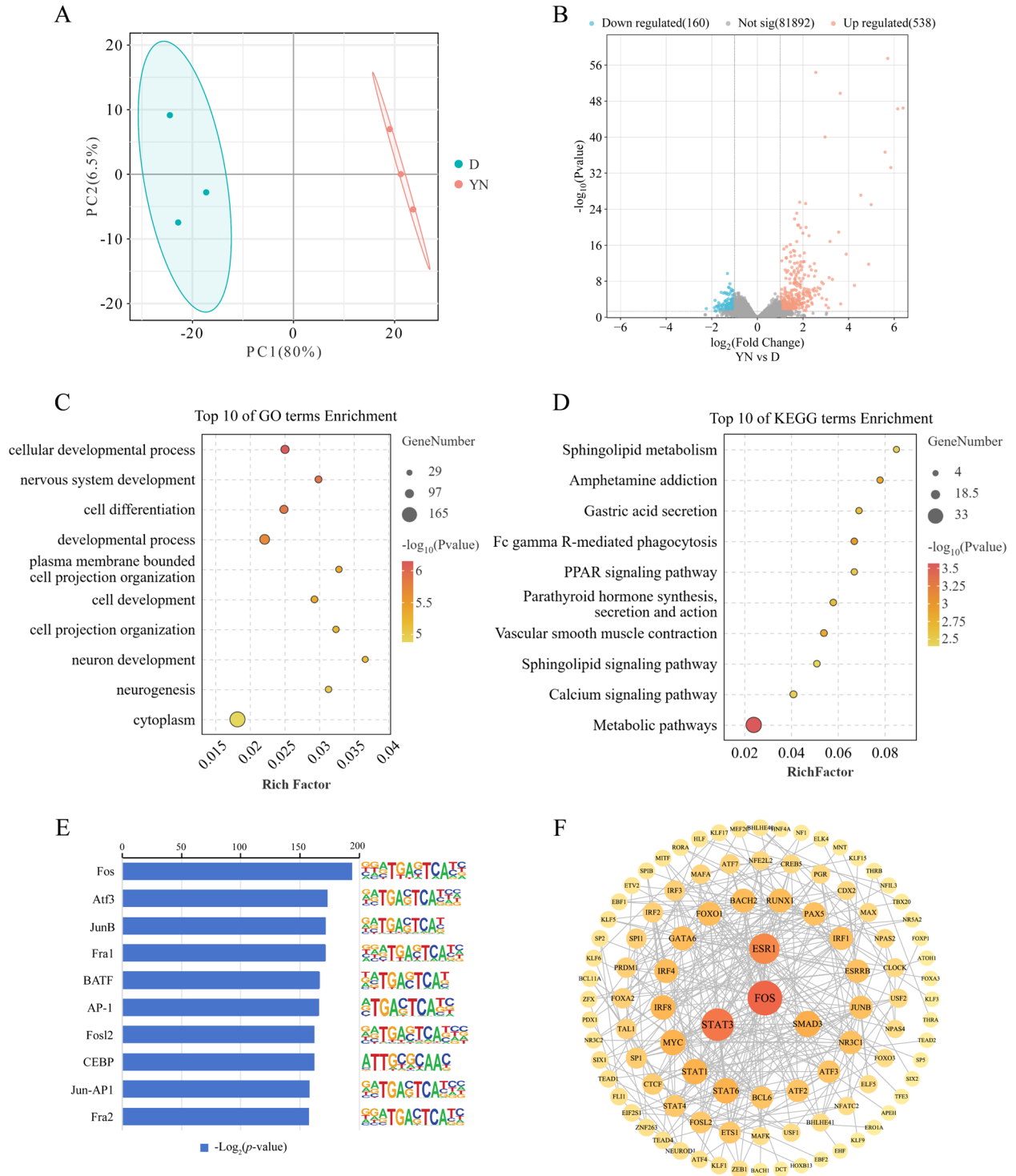

Fig. 3 Differential peaks and corresponding gene enrichment analysis. **A** Principal component analysis (PCA). **B** Volcanic map of differential peaks. **C** GO enrichment analysis of genes linked to differential peaks. **D** KEGG pathway enrichment analysis of genes linked to differential peaks. **E** Top 10 TFs enriched in motifs of differential peaks. **F** TF interaction network. Node size and color indicate the number of connections to other TFs

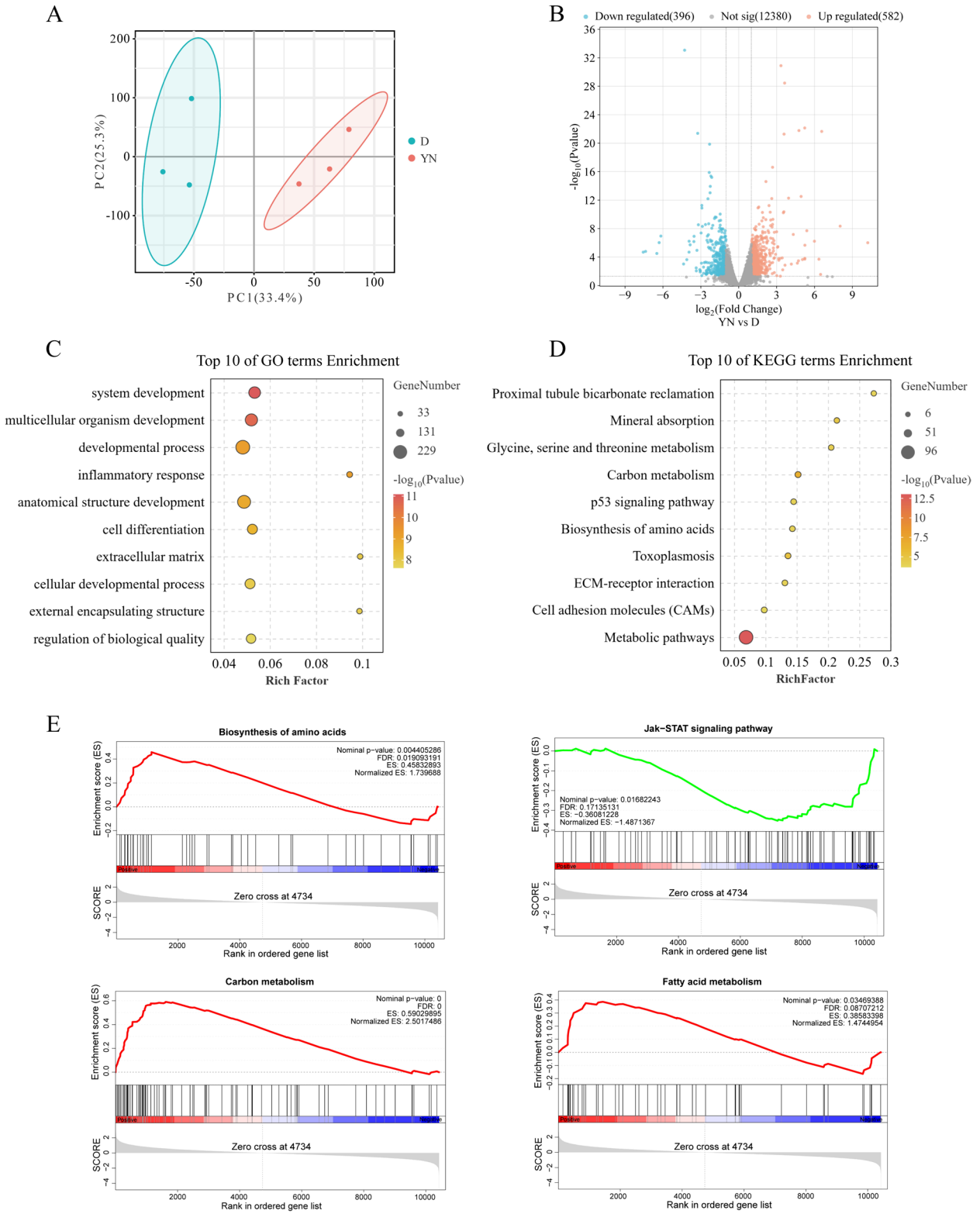

Fig. 4 Analyses of RNA-seq. **A** PCA. **B** Volcanic map of DEGs. **C** GO enrichment analysis of DEGs. **D** KEGG pathway enrichment analysis of DEGs. **E** Pathway identified by GSEA

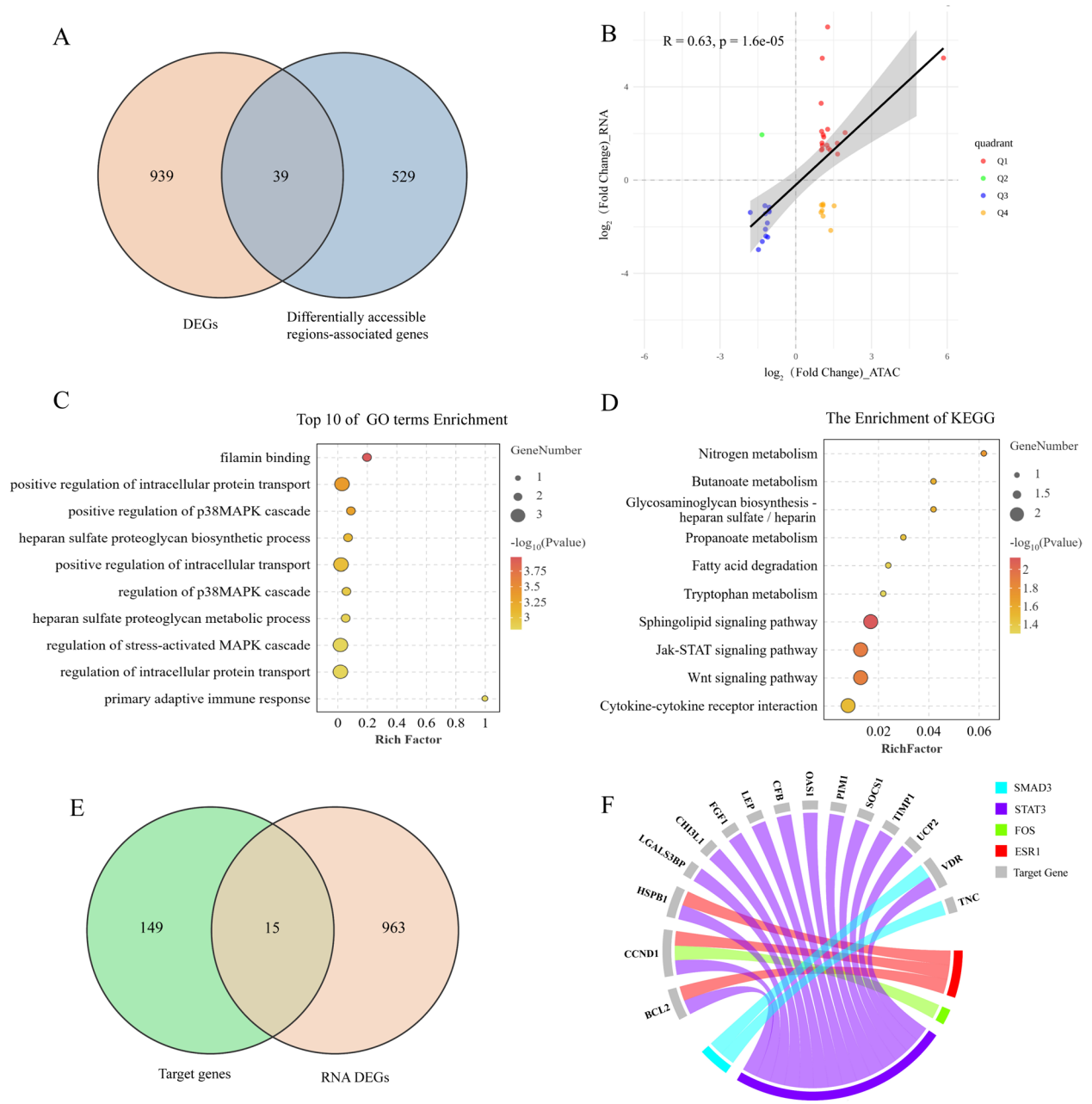

Fig. 5 Analysis of integrated ATAC-seq and RNA-seq results. **A** Overlap of differential genes identified by ATAC-seq and RNA-seq. **B** Analysis of correlation between gene expression level and chromatin accessibility. **C** GO enrichment analysis of overlapping differential genes. **D** KEGG pathway enrichment analysis of overlapping differential genes. **E** Overlap of SMAD3, STAT3, FOS, and ESR1 target genes with DEGs identified by RNA-seq. **F** The regulatory network of SMAD3, STAT3, FOS and ESR1 with their corresponding target genes

Discussion

The study of backfat tissues in YN and D allows for a deeper understanding of the genetic characteristics and gene expression patterns in these two pig breeds, which helps breeders selectively cultivate economically viable pig breeds that cater to market demands. ATAC-seq, a widely utilized high-throughput sequencing method, is employed for examining open chromatin regions across the genome. Furthermore, it can be used to investigate transcriptional regulatory elements such as promoters, silencers and enhancers in the genome, revealing the structure and function of gene regulatory networks and identifying potential active TFs and their target genes [11]. While RNA-seq can reveal the transcriptional status

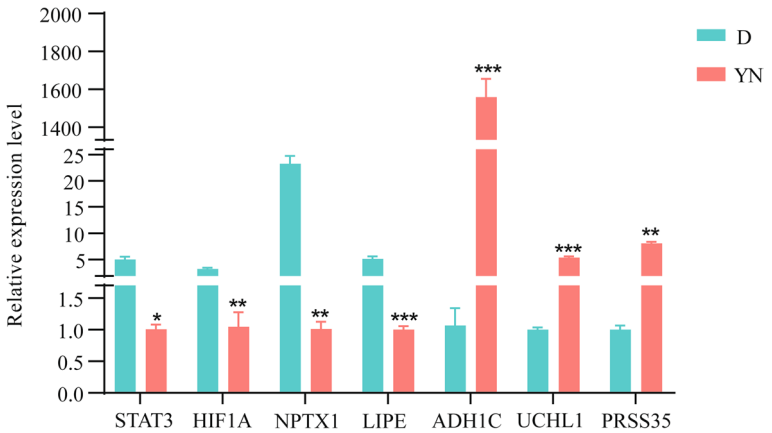

Fig. 6 Verification of RNA-seq data by RT-qPCR. The y-axis displays the relative expression levels measured by RT-qPCR. mean ± SD, * $P < 0.05$, ** $P < 0.01$, *** $P < 0.001$

of TFs and genes [25]. Therefore, TFs and genes that may regulate backfat deposition could be identified through ATAC-seq and RNA-seq analysis of backfat tissues in YN and D.

In the present study, a comprehensive analysis utilizing ATAC-seq identified 568 genes from 698 regions exhibiting differential accessibility in the backfat tissues of YN and D groups. Complementarily, RNA-seq analysis revealed 978 DEGs. Subsequent KEGG pathway enrichment analysis highlighted the enrichment of these genes in pathways pertinent to fat deposition, cell proliferation, differentiation, as well as fatty acid and glycolipid metabolism, including Metabolic pathways, PPAR signaling pathway, Sphingolipid metabolism, p53 signaling pathway, ECM-receptor interaction, Carbon metabolism, and Biosynthesis of amino acids [26–34]. Interestingly, GSEA analysis also significantly enriched Biosynthesis of amino acids and Carbon metabolism pathways, emphasizing their significance in adipogenesis. Integrating ATAC-seq and RNA-seq data, 39 genes with differences in chromatin accessibility and expression levels were identified. Correlation analysis underscored a strong relation between the chromatin accessibility of these genes and their expression levels. KEGG pathway enrichment analysis illuminated their involvement in pathways crucial for fat deposition, such as the Wnt signaling pathway, Jak-STAT signaling pathway, and Fatty acid degradation pathway. The Wnt signaling pathway plays a crucial role in the regulation of adipogenesis [35, 36]. Specifically, the Wnt signaling pathway can reduce adipogenesis by inhibiting adipogenic TFs like CCAAT/enhancer binding protein alpha (C/EBPα) and peroxisome proliferator-activated receptor gamma (PPARγ) [37]. Its role extends to governing body fat distribution, obesity, and metabolic functions [38]. *CTBP2* and *TCF7L2* are involved in the Wnt signaling pathway. CTBP2, acting as a transcriptional repressor, forms a transcriptional repressor complex with KLF3 to suppress the expression of key adipogenic regulators including C/EBPα and PPARγ [39, 40]. TCF7L2, a key transcriptional effector in the adipogenesis process regulated by the Wnt signaling pathway, plays a critical role in the regulation of lipid metabolism [41, 42], adipocyte size and glucose metabolism in adipose tissue, with its conditional deletion leading to insulin insensitivity, lipid metabolic disorders, and adipocyte hypertrophy [43, 44]. The Jak-STAT signaling pathway controls both adipose tissue development and adipogenesis by affecting various cytokines, growth factors, and hormones [45]. Specifically, it participates in the regulation of adipogenesis by controlling the transcription of CCAAT/enhancer-binding protein beta (C/EBPβ) [46]. Additionally, Btg2, a member of the anti-proliferative protein family, has an inhibitory effect on adipogenesis, suppressed by the activation of the Jak-STAT signaling pathway [47]. *LEP* and *OSMR* are involved in the Jak-STAT signaling pathway. Leptin, encoded by *LEP* and primarily secreted by adipose tissue, is an adipocyte-derived hormone crucial for lipolysis [48], regulating energy balance by acting on both the central nervous system and peripheral tissues [49, 50], while also modulating the levels of fat deposition by controlling ATGL mRNA and protein expression through the Jak-STAT signaling pathway [48]. Notably, the concentration of leptin is positively correlated with fat mass, aligning with the findings of this research [51]. The OSM receptor, encoded by *OSMR* and highly expressed in fat tissue [52, 53], regulates the homeostasis of adipose tissue by inhibiting adipogenesis through the OSM-OSMR signaling [54–56]. Fatty acids are important chemical substances within adipose tissue, stored as triglycerides within adipocytes [57]. The fatty acid degradation

pathway promotes fat oxidation, thereby reducing lipid levels and preventing fat accumulation [58, 59]. Consequently, this pathway is essential for maintaining energy balance and combating obesity. *EHHADH* encodes a multifunctional enzyme crucial in the peroxisomal beta-oxidation pathway and is closely linked to glucose and lipid metabolism [60, 61]. Recent research has suggested that *EHHADH* functions as a negative regulator of triglyceride synthesis, with its overexpression resulting in reduced intracellular triglyceride levels [62].

Adipogenesis is regulated by numerous TFs [63]. Open chromatin regions offer binding sites for TFs, thereby regulating the transcription levels of target genes. The current study reveals a compelling correlation between gene expression levels and chromatin accessibility, indicating that these genes may be regulated by associated TFs, indicating that these genes may be regulated by associated TFs. Differential chromatin accessibility regions are enriched with several key TFs, including FOS, STAT3, ESR1, and SMAD3. FOS, a member of the FOS gene family, is involved in adipocyte differentiation [64]. Research by Hu et al. demonstrated that FOS inhibits intramuscular fat formation in goats and may negatively regulate the expression of C/EBPβ, C/EBPα, and PPARγ [65]. Another study revealed that FOS knockout in 3T3-L1 adipocytes reduced lipid droplet accumulation and inhibited adipocyte differentiation [64]. STAT3, a TF involved in regulating immune responses, cell survival, and the cell cycle, is highly expressed in adipocytes and mediates the effects of various cytokines [45, 66]. It is regulated both endogenously and exogenously by adipocytes and vigorously activated during the proliferation phase of 3T3-L1 preadipocytes, playing a crucial role in adipocyte proliferation [67]. Early in the adipogenesis process, STAT3 binds to the distal region of the C/EBPβ promoter, regulating its transcription level and thereby contributing to adipogenesis [46]. Additionally, STAT3 participates in the activation of PPARγ, further exerting its influence on the adipogenesis process [68]. ESR1, inversely associated with fat mass, encodes estrogen receptor α (Erα), a protein instrumental in regulating mitochondrial function and energy homeostasis in adipocytes [69]. SMAD3 is indispensable for the formation and maintenance of white adipose tissue [70]. It inhibits the transcription of C/EBP, thereby suppressing adipocyte differentiation [71]. Studies have shown that SMAD3 knockout mice exhibit impaired lipid biosynthesis and fat deposition, which can protect against obesity induced by high-fat diets [72].

Further analysis identified 15 target genes of these TFs that exhibited differential expression between the D and YN groups, many of which are pivotal in lipid metabolism, energy metabolism, and adipocyte differentiation, including *LEP*, *BCL2*, *FGF1*, and *UCP2*, etc. *BCL2* serves as an anti-apoptotic factor, inhibiting cell apoptosis [73]. Studies have demonstrated that conjugated linoleic acid can promote adipocyte apoptosis by reducing the expression of the *BCL2* in porcine backfat, thereby decreasing fat deposition [74]. *FGF1*, an important adipogenic factor, facilitates the proliferation and differentiation of preadipocytes. It promotes adipogenesis via the FGF-1/FGF receptor 1/fibroblast growth factor receptor substrate 2 (FRS2)/mitogen-activated protein kinase (MAPK) pathway [75]. *UCP2* encodes uncoupling protein 2, crucial for cellular energy metabolism and mainly found in the pancreas, central nervous system, and white adipose tissue [76]. Studies have found that *UCP2* deficiency in mice protects against high-fat diet-induced obesity modulating adipocyte apoptosis [77]. *CCND1* encodes cyclin D1, a key regulator of cell cycle progression. Liu et al. discovered that knocking down *ZFP217* reduced the expression of the *CCND1* gene and protein, subsequently hindering the cell cycle and adipogenesis [78]. *TIMP1* acts as an inhibitor during adipogenesis, and specifically knocking down chemerin in subcutaneous adipose tissue promotes adipogenesis by down-regulating *TIMP1* [79, 80]. *VDR* is pivotal in the regulation of energy homeostasis in adipose tissue. Mice lacking *VDR* exhibit reduced energy expenditure, while *VDR* over-expression leads to increased energy expenditure [81]. As the receptor for 1,25-dihydroxyvitamin D3 (1,25(OH)2D3), VDR is crucial in the 1,25(OH)2D3-mediated adipogenesis process. It has been reported that 1,25(OH)2D3 inhibits adipogenesis through the regulation of C/EBPβ and PPARγ expression [82]. Overall, relevant studies have substantiated the critical biological functions of the aforementioned genes, TFs, and pathways, particularly highlighting their roles in adipose deposition. Furthermore, integrated RNA-seq and ATAC-seq analyses reveal a positive correlation between gene expression levels and chromatin accessibility for most genes, while other genes exhibit the opposite effect. This discrepancy may be attributed to transcriptional repressors binding to open chromatin regions, or the influence of DNA methylation and other epigenetic modifications in these areas [14, 83]. Future studies are warranted to clarify the epigenetic processes by which specific TFs and their corresponding binding sites regulate the transcription of associated genes.

This study combines ATAC-seq and RNA-seq to conduct a systematic investigation of the molecular mechanisms underlying porcine backfat deposition from both epigenetic and gene expression regulatory perspectives. It identifies potential TFs and genes influencing porcine backfat deposition, shedding new light on the complex

regulatory network of fat deposition and laying the foundation for further exploration of the molecular mechanisms underlying backfat deposition in pigs.

Conclusion

In summary, this study utilized ATAC-seq and RNA-seq to delve into chromatin accessibility and gene expression in the backfat tissue of YN and D at a genome-wide scale, identifying and predicting key genes, TFs, and pathways involved in backfat deposition. Integrated analysis of ATAC-seq and RNA-seq data revealed 11 potential candidate genes (*LEP*, *CTBP2*, *EHHADH*, *OSMR*, *TCF7L2*, *BCL2*, *FGF1*, *UCP2*, *CCND1*, *TIMP1*, and *VDR*) and three pathways (Wnt signaling pathway, Jak-STAT signaling pathway, and Fatty acid degradation). Additionally, the regulatory network of TF-TF and TF-target gene interactions were established, and four TFs (FOS, STAT3, SMAD3, and ESR1) were suggested to potentially have significant roles in backfat deposition. The identification of these candidate genes, TFs and pathways represents a significant advancement in understanding the regulatory mechanisms underlying backfat deposition, thereby offering valuable insights for devising genetic improvement strategies in pig breeding and advancing the livestock industry.

Supplementary Information

The online version contains supplementary material available at https://doi.org/10.1186/s12864-024-10805-1.

Supplementary Material 1.

Acknowledgements
Not applicable.

Authors' contributions
Conceptualization, Z.Z. and X.H.; methodology, Z.Z., L.C. and B.W.; validation, Z.Z., L.C., B.W. and Y.W.; formal analysis, Z.Z., L.C. and B.W.; investigation, Z.Z., L.C. and B.W.; resources, Y.Z., X.L. (Xinjian Li) and X.L. (Xiuling Li); data curation, K.W.; writing—original draft preparation, Z.Z.; writing—review and editing, Z.Z. and X.H.; visualization, Z.Z.; supervision, R.Q., F.Y. and T.Y.; project administration, X.H.; funding acquisition, X.H. All authors have read and agreed to the published version of the manuscript.

Funding
This research was funded by Biological Breeding-Major Projects in National Science and Technology (2023ZD0404604), the 14th Five-Year National Key R&D Program (2021YFD1301202), and the Agricultural Breeds Research Project of Henan Province (2022020101).

Availability of data and materials
All raw data of high-throughput sequencing have been deposited to the National Genomics Data Center (NGDC, https://bigd.big.ac.cn) with the dataset accession number CRA017961.

Declarations

Ethics approval and consent to participate
All animal experiments were conducted following the guidelines for the care and use of experimental animals established by the Ministry of Science and Technology of the People's Republic of China (Approval Number DWLL20211193). The Ethics Committee of Henan Agricultural University reviewed and approved the animal study. Furthermore, all procedures related to slaughter, sampling, and sample preservation were performed in compliance with the relevant approved guidelines and regulations. All animal experiments involving pigs in this study were conducted with the informed consent of the owners. Clinical trial number: not applicable.

Consent for publication
Not applicable.

Competing interests
The authors declare no competing interests.

Received: 22 July 2024 Accepted: 17 September 2024
Published online: 30 September 2024

References

1. Choe SS, Huh JY, Hwang IJ, Kim JI, Kim JB. Adipose tissue remodeling: its role in energy metabolism and metabolic disorders. Front Endocrinol (Lausanne). 2016;7:30.
2. Yamamoto A, Kikuchi Y, Kusakabe T, Takano H, Sakurai K, Furui S, Oba H. Imaging spectrum of abnormal subcutaneous and visceral fat distribution. Insights Imaging. 2020;11(1):24.
3. Jo J, Gavrilova O, Pack S, Jou W, Mullen S, Sumner AE, Cushman SW, Periwal V. Hypertrophy and/or Hyperplasia: dynamics of adipose tissue growth. PLoS Comput Biol. 2009;5(3): e1000324.
4. Cristancho AG, Lazar MA. Forming functional fat: a growing understanding of adipocyte differentiation. Nat Rev Mol Cell Biol. 2011;12(11):722–34.
5. Faust IM, Johnson PR, Stern JS, Hirsch J. Diet-induced adipocyte number increase in adult rats: a new model of obesity. Am J Physiol. 1978;235(3):E279-286.
6. Xing K, Zhu F, Zhai L, Chen S, Tan Z, Sun Y, Hou Z, Wang C. Identification of genes for controlling swine adipose deposition by integrating transcriptome, whole-genome resequencing, and quantitative trait loci data. Sci Rep. 2016;6: 23219.
7. Xue Y, Li C, Duan D, Wang M, Han X, Wang K, Qiao R, Li XJ, Li XL. Genome-wide association studies for growth-related traits in a crossbreed pig population. Anim Genet. 2021;52(2):217–22.
8. Zhang D, Deng Y, Kukanja P, Agirre E, Bartosovic M, Dong M, Ma C, Ma S, Su G, Bao S, et al. Spatial epigenome-transcriptome co-profiling of mammalian tissues. Nature. 2023;616(7955):113–22.
9. Tsompana M, Buck MJ. Chromatin accessibility: a window into the genome. Epigenetics Chromatin. 2014;7(1): 33.
10. Yan F, Powell DR, Curtis DJ, Wong NC. From reads to insight: a hitchhiker's guide to ATAC-seq data analysis. Genome Biol. 2020;21(1):22.
11. Grandi FC, Modi H, Kampman L, Corces MR. Chromatin accessibility profiling by ATAC-seq. Nat Protoc. 2022;17(6):1518–52.
12. Chen G, Liu Z, Li S, Liu L, Lu L, Wang Z, Mendu V, Li F, Yang Z. Characterization of chromatin accessibility and gene expression reveal the key genes involved in cotton fiber elongation. Physiol Plant. 2023;175(4): e13972.
13. Miao W, Ma Z, Tang Z, Yu L, Liu S, Huang T, Wang P, Wu T, Song Z, Zhang H, et al. Integrative ATAC-seq and RNA-seq analysis of the Longissimus muscle of Luchuan and Duroc pigs. Front Nutr. 2021;8: 742672.
14. Zhang Z, Zhang Y, Bao Q, Gu Y, Liang C, Chu M, Guo X, Bao P, Yan P. The Landscape of Accessible chromatin during Yak Adipocyte differentiation. Int J Mol Sci 2022, 23(17):9960.
15. Xu Z, Wu J, Zhou J, Zhang Y, Qiao M, Sun H, Li Z, Li L, Chen N, Oyelami FO, et al. Integration of ATAC-seq and RNA-seq analysis identifies key genes affecting intramuscular fat content in pigs. Front Nutr. 2022;9:1016956.
16. Schneider CA, Rasband WS, Eliceiri KW. NIH Image to ImageJ: 25 years of image analysis. Nat Methods. 2012;9(7):671–5.
17. Buenrostro JD, Wu B, Chang HY, Greenleaf WJ. ATAC-seq: A Method for Assaying Chromatin Accessibility Genome-Wide. Current protocols in molecular biology 2015, 109:21.29.21–21.29.29.
18. Langmead B, Salzberg SL. Fast gapped-read alignment with Bowtie 2. Nat Methods. 2012;9(4):357–9.

19. Zhang Y, Liu T, Meyer CA, Eeckhoute J, Johnson DS, Bernstein BE, Nusbaum C, Myers RM, Brown M, Li W, et al. Model-based analysis of ChIP-Seq (MACS). Genome Biol. 2008;9(9):R137.
20. Yu G, Wang LG, He QY. ChIPseeker: an R/Bioconductor package for ChIP peak annotation, comparison and visualization. Bioinf (Oxford England). 2015;31(14):2382–3.
21. Ross-Innes CS, Stark R, Teschendorff AE, Holmes KA, Ali HR, Dunning MJ, Brown GD, Gojis O, Ellis IO, Green AR, et al. Differential oestrogen receptor binding is associated with clinical outcome in breast cancer. Nature. 2012;481(7381):389–93.
22. Shannon P, Markiel A, Ozier O, Baliga NS, Wang JT, Ramage D, Amin N, Schwikowski B, Ideker T. Cytoscape: a software environment for integrated models of biomolecular interaction networks. Genome Res. 2003;13(11):2498–504.
23. Kim D, Paggi JM, Park C, Bennett C, Salzberg SL. Graph-based genome alignment and genotyping with HISAT2 and HISAT-genotype. Nat Biotechnol. 2019;37(8):907–15.
24. Love MI, Huber W, Anders S. Moderated estimation of Fold change and dispersion for RNA-seq data with DESeq2. Genome Biol. 2014;15(12):550.
25. Wang Z, Gerstein M, Snyder M. RNA-Seq: a revolutionary tool for transcriptomics. Nat Rev Genet. 2009;10(1):57–63.
26. Evans RM, Barish GD, Wang YX. PPARs and the complex journey to obesity. Nat Med. 2004;10(4):355–61.
27. Worgall TS. Regulation of lipid metabolism by sphingolipids. Subcell Biochem. 2008;49:371–85.
28. Meikle PJ, Summers SA. Sphingolipids and phospholipids in insulin resistance and related metabolic disorders. Nat Reviews Endocrinol. 2017;13(2):79–91.
29. Liu S, Kim TH, Franklin DA, Zhang Y. Protection against high-fat-diet-induced obesity in MDM2(C305F) mice due to reduced p53 activity and enhanced energy expenditure. Cell Rep. 2017;18(4):1005–18.
30. Lee HJ, Jang M, Kim H, Kwak W, Park W, Hwang JY, Lee CK, Jang GW, Park MN, Kim HC, et al. Comparative transcriptome analysis of adipose tissues reveals that ECM-Receptor Interaction is involved in the Depot-specific adipogenesis in cattle. PLoS ONE. 2013;8(6): e66267.
31. Jiang S, Wei H, Song T, Yang Y, Peng J, Jiang S. Transcriptome comparison between porcine subcutaneous and intramuscular stromal vascular cells during adipogenic differentiation. PLoS ONE. 2013;8(10): e77094.
32. Du Y, Meng Q, Zhang Q, Guo F. Isoleucine or valine deprivation stimulates fat loss via increasing energy expenditure and regulating lipid metabolism in WAT. Amino Acids. 2012;43(2):725–34.
33. Moura CS, Lollo PCB, Morato PN, Risso EM, Amaya-Farfan J. Modulatory effects of arginine, glutamine and branched-chain amino acids on heat shock proteins, immunity and antioxidant response in exercised rats. Food Funct. 2017;8(9):3228–38.
34. Calejman CM, Doxsey WG, Fazakerley DJ, Guertin DA. Integrating adipocyte insulin signaling and metabolism in the multi-omics era. Trends Biochem Sci. 2022;47(6):531–46.
35. Song K, Wang S, Mani M, Mani A. Wnt signaling, de novo lipogenesis, adipogenesis and ectopic fat. Oncotarget. 2014;5(22):11000–3.
36. Huh JE, Choi JY, Shin YO, Park DS, Kang JW, Nam D, Choi DY, Lee JD. Arginine enhances osteoblastogenesis and inhibits adipogenesis through the regulation of wnt and NFATc signaling in human mesenchymal stem cells. Int J Mol Sci. 2014;15(7):13010–29.
37. Ross SE, Hemati N, Longo KA, Bennett CN, Lucas PC, Erickson RL, MacDougald OA. Inhibition of adipogenesis by wnt signaling. Sci (New York NY). 2000;289(5481):950–3.
38. Bagchi DP, MacDougald OA. Wnt signaling: from mesenchymal cell fate to Lipogenesis and other mature adipocyte functions. Diabetes. 2021;70(7):1419–30.
39. Kajimura S, Seale P, Tomaru T, Erdjument-Bromage H, Cooper MP, Ruas JL, Chin S, Tempst P, Lazar MA, Spiegelman BM. Regulation of the brown and white fat gene programs through a PRDM16/CtBP transcriptional complex. Genes Dev. 2008;22(10):1397–409.
40. Han JH, Jang KW, Myung CS. Garcinia cambogia attenuates adipogenesis by affecting CEBPB and SQSTM1/p62-mediated selective autophagic degradation of KLF3 through RPS6KA1 and STAT3 suppression. Autophagy. 2022;18(3):518–39.
41. Yang H, Li Q, Lee JH, Shu Y. Reduction in Tcf7l2 expression decreases diabetic susceptibility in mice. Int J Biol Sci. 2012;8(6):791–801.
42. Chen X, Ayala I, Shannon C, Fourcaudot M, Acharya NK, Jenkinson CP, Heikkinen S, Norton L. The diabetes gene and wnt pathway Effector TCF7L2 regulates adipocyte development and function. Diabetes. 2018;67(4):554–68.
43. Nguyen-Tu MS, Martinez-Sanchez A, Leclerc I, Rutter GA, da Silva Xavier G. Adipocyte-specific deletion of Tcf7l2 induces dysregulated lipid metabolism and impairs glucose tolerance in mice. Diabetologia. 2021;64(1):129–41.
44. Geoghegan G, Simcox J, Seldin MM, Parnell TJ, Stubben C, Just S, Begaye L, Lusis AJ, Villanueva CJ. Targeted deletion of Tcf7l2 in adipocytes promotes adipocyte hypertrophy and impaired glucose metabolism. Mol Metabolism. 2019;24:44–63.
45. Richard AJ, Stephens JM. The role of JAK-STAT signaling in adipose tissue function. Biochim Biophys Acta. 2014;1842(3):431–9.
46. Zhang K, Guo W, Yang Y, Wu J. JAK2/STAT3 pathway is involved in the early stage of adipogenesis through regulating C/EBPβ transcription. J Cell Biochem. 2011;112(2):488–97.
47. Kim S, Hong JW, Park KW. B cell translocation gene 2 (Btg2) is regulated by Stat3 signaling and inhibits adipocyte differentiation. Mol Cell Biochem. 2016;413(1–2):145–53.
48. Li YC, Zheng XL, Liu BT, Yang GS. Regulation of ATGL expression mediated by leptin in vitro in porcine adipocyte lipolysis. Mol Cell Biochem. 2010;333(1–2):121–8.
49. Park HK, Ahima RS. Physiology of leptin: energy homeostasis, neuroendocrine function and metabolism. Metab Clin Exp. 2015;64(1):24–34.
50. Burguera B, Couce ME, Curran GL, Jensen MD, Lloyd RV, Cleary MP, Poduslo JF. Obesity is associated with a decreased leptin transport across the blood-brain barrier in rats. Diabetes. 2000;49(7):1219–23.
51. Schwartz MW, Peskind E, Raskind M, Boyko EJ, Porte D Jr. Cerebrospinal fluid leptin levels: relationship to plasma levels and to adiposity in humans. Nat Med. 1996;2(5):589–93.
52. Komori T, Tanaka M, Senba E, Miyajima A, Morikawa Y. Deficiency of oncostatin M receptor β (OSMRβ) exacerbates high-fat diet-induced obesity and related metabolic disorders in mice. J Biol Chem. 2014;289(20):13821–37.
53. Sanchez-Infantes D, White UA, Elks CM, Morrison RF, Gimble JM, Considine RV, Ferrante AW, Ravussin E, Stephens JM. Oncostatin m is produced in adipose tissue and is regulated in conditions of obesity and type 2 diabetes. J Clin Endocrinol Metab. 2014;99(2):E217-225.
54. Miyaoka Y, Tanaka M, Naiki T, Miyajima A. Oncostatin M inhibits adipogenesis through the RAS/ERK and STAT5 signaling pathways. J Biol Chem. 2006;281(49):37913–20.
55. Elks CM, Zhao P, Grant RW, Hang H, Bailey JL, Burk DH, McNulty MA, Mynatt RL, Stephens JM. Loss of oncostatin M signaling in adipocytes induces insulin resistance and adipose tissue inflammation in vivo. J Biol Chem. 2016;291(33):17066–76.
56. Stephens JM, Bailey JL, Hang H, Rittell V, Dietrich MA, Mynatt RL, Elks CM. Adipose tissue dysfunction occurs independently of obesity in adipocyte-specific oncostatin receptor knockout mice. Obes (Silver Spring Md). 2018;26(9):1439–47.
57. Cho CH, Patel S, Rajbhandari P. Adipose tissue lipid metabolism: lipolysis. Curr Opin Genet Dev. 2023;83: 102114.
58. Frayn KN, Arner P, Yki-Järvinen H. Fatty acid metabolism in adipose tissue, muscle and liver in health and disease. Essays Biochem. 2006;42:89–103.
59. He S, Xiong Z, Li L, Wang Y, Wang C, Zheng B, Zeng H, Zhang Y. Lotus seed resistant starch ameliorates high-fat diet induced hyperlipidemia by fatty acid degradation and glycerolipid metabolism pathways in mouse liver. Int J Biol Macromol. 2022;215:79–91.
60. Wang C, Hu M, Yi Y, Wen X, Lv C, Shi M, Zeng C. Multiomic analysis of dark tea extract on glycolipid metabolic disorders in db/db mice. Front Nutr. 2022;9: 1006517.
61. Liu H, Sun W, Zhou Y, Griffin N, Faulkner S, Wang L. iTRAQ-based quantitative proteomics analysis of Sprague-Dawley rats liver reveals perfluorooctanoic acid-induced lipid metabolism and urea cycle dysfunction. Toxicol Lett. 2022;357:20–32.
62. Li G, Yang R, Lu X, Liu Y, He W, Li Y, Yu H, Qin L, Cao Y, Zhao Z, et al. RNA-Seq analysis identifies differentially expressed genes in the longissimus dorsi of Wagyu and chinese red steppe cattle. Int J Mol Sci. 2022;24(1):387.
63. White UA, Stephens JM. Transcriptional factors that promote formation of white adipose tissue. Mol Cell Endocrinol. 2010;318(1–2):10–4.
64. Xiao H, Leblanc SE, Wu Q, Konda S, Salma N, Marfella CG, Ohkawa Y, Imbalzano AN. Chromatin accessibility and transcription factor binding at the PPARγ2 promoter during adipogenesis is protein kinase A-dependent. J Cell Physiol. 2011;226(1):86–93.

65. Hu T, Li Z, Gong C, Xiong Y, Sun S, Xing J, Li Y, Li R, Wang Y, Wang Y, et al. FOS inhibits the differentiation of intramuscular adipocytes in goats. Genes. 2023;14(11):2088.
66. Butturini E, Carcereri de Prati A, Mariotto S. Redox Regulation of STAT1 and STAT3 signaling. Int J Mol Sci 2020, 21(19):7034.
67. Deng J, Hua K, Lesser SS, Harp JB. Activation of signal transducer and activator of transcription-3 during proliferative phases of 3T3-L1 adipogenesis. Endocrinology. 2000;141(7):2370–6.
68. Wang D, Zhou Y, Lei W, Zhang K, Shi J, Hu Y, Shu G, Song J. Signal transducer and activator of transcription 3 (STAT3) regulates adipocyte differentiation via peroxisome-proliferator-activated receptor gamma (PPARgamma). Biol Cell. 2009;102(1):1–12.
69. Zhou Z, Moore TM, Drew BG, Ribas V, Wanagat J, Civelek M, Segawa M, Wolf DM, Norheim F, Seldin MM et al: Estrogen receptor α controls metabolism in white and brown adipocytes by regulating Polg1 and mitochondrial remodeling. Science translational medicine 2020, 12(555):eaax8096.
70. Kumari R, Irudayam MJ, Al Abdallah Q, Jones TL, Mims TS, Puchowicz MA, Pierre JF, Brown CW. SMAD2 and SMAD3 differentially regulate adiposity and the growth of subcutaneous white adipose tissue. FASEB Journal: Official Publication Federation Am Soc Experimental Biology. 2021;35(12):e22018.
71. Choy L, Derynck R. Transforming growth factor-beta inhibits adipocyte differentiation by Smad3 interacting with CCAAT/enhancer-binding protein (C/EBP) and repressing C/EBP transactivation function. J Biol Chem. 2003;278(11):9609–19.
72. Tan CK, Leuenberger N, Tan MJ, Yan YW, Chen Y, Kambadur R, Wahli W, Tan NS. Smad3 deficiency in mice protects against insulin resistance and obesity induced by a high-fat diet. Diabetes. 2011;60(2):464–76.
73. Gross A, McDonnell JM, Korsmeyer SJ. BCL-2 family members and the mitochondria in apoptosis. Genes Dev. 1999;13(15):1899–911.
74. Qi R, Yang F, Huang J, Peng H, Liu Y, Liu Z. Supplementation with conjugated linoeic acid decreases pig back fat deposition by inducing adipocyte apoptosis. BMC Vet Res. 2014;10: 141.
75. Widberg CH, Newell FS, Bachmann AW, Ramnoruth SN, Spelta MC, Whitehead JP, Hutley LJ, Prins JB. Fibroblast growth factor receptor 1 is a key regulator of early adipogenic events in human preadipocytes. Am J Physiol Endocrinol Metabolism. 2009;296(1):E121-131.
76. da Fonseca ACP, Assis I, Salum KCR, Palhinha L, Abreu GM, Zembrzuski VM, Campos Junior M, Nogueira-Neto JF, Cambraia A, Souza Junior MLF, et al. Genetic variants in DBC1, SIRT1, UCP2 and ADRB2 as potential biomarkers for severe obesity and metabolic complications. Front Genet. 2024;15:1363417.
77. Kim DH, Kim HJ, Seong JK. UCP2 KO mice exhibit ameliorated obesity and inflammation induced by high-fat diet feeding. BMB Rep. 2022;55(10):500–5.
78. Liu Q, Zhao Y, Wu R, Jiang Q, Cai M, Bi Z, Liu Y, Yao Y, Feng J, Wang Y, et al. ZFP217 regulates adipogenesis by controlling mitotic clonal expansion in a METTL3-m(6)a dependent manner. RNA Biol. 2019;16(12):1785–93.
79. Meissburger B, Stachorski L, Röder E, Rudofsky G, Wolfrum C. Tissue inhibitor of matrix metalloproteinase 1 (TIMP1) controls adipogenesis in obesity in mice and in humans. Diabetologia. 2011;54(6):1468–79.
80. Huang CL, Xiao LL, Xu M, Li J, Li SF, Zhu CS, Lin YL, He R, Li X. Chemerin deficiency regulates adipogenesis is depot different through TIMP1. Genes Dis. 2021;8(5):698–708.
81. Wong KE, Kong J, Zhang W, Szeto FL, Ye H, Deb DK, Brady MJ, Li YC. Targeted expression of human vitamin D receptor in adipocytes decreases energy expenditure and induces obesity in mice. J Biol Chem. 2011;286(39):33804–10.
82. Salehpour A, Hedayati M, Shidfar F, Neshatbini Tehrani A, Farshad AA, Mohammadi S. 1,25-Dihydroxyvitamin D3 modulates adipogenesis of human adipose-derived mesenchymal stem cells dose-dependently. Nutr Metab. 2021;18(1):29.
83. Truskina J, Han J, Chrysanthou E, Galvan-Ampudia CS, Lainé S, Brunoud G, Macé J, Bellows S, Legrand J, Bågman AM, et al. A network of transcriptional repressors modulates auxin responses. Nature. 2021;589(7840):116–9.

Publisher's note